Optical Variability and Bottom Classification in Turbid Waters: HyMOM Predictions of the Light Field in Ports and Beneath Ship Hulls

Kendall L. Carder
University of South Florida, College of Marine Science
140 7th Avenue South, St. Petersburg, FL 33701
phone: 727-553-3952 FAX: 727-553-3918 email: kcarder@monty.marine.usf.edu

Phillip N. Reinersman
University of South Florida, College of Marine Science
140 7th Avenue South, St. Petersburg, FL 33701
phone: 727-553-3952 FAX: 727-553-3918 email: flip@monty.marine.usf.edu

Award Number: N00014-02-1-0211

LONG-TERM GOALS

The long-term goal of this research effort is to develop a method to predict the visible and ultraviolet radiance distribution in complex three-dimensional marine environments as found in ports, anchorages, and coastal waters. Effective deployment of AUV- or ROV-mounted sensors to inspect ship hulls and port facilities will depend on accurate, real-time prediction of the sub-surface optical environment at the time and place of inspection. Furthermore, since the active or passive camouflaging of divers, AUVs, and bottom objects is quite dependent upon masking the effects of three-dimensionality, 3-D optical models to evaluate such problems are being developed and implemented. While HyMOM will be used to calculate light fluxes to the bottom for foreign-object detection near structures such as coral heads, seawalls, and pilings, it is equally useful in ecological models dealing with the bleaching of corals and foraminifera and the photosynthesis of benthic plants.

OBJECTIVES

The initial objective of this work is to extend the existing model system from two-dimensional environments into realistic three-dimensional environments. The model concept involves four distinct phases: 1) Modeling the optical response of individual three-dimensional elements using Monte Carlo techniques, analytic expressions, and ad-hoc definitions; 2) Building the three-dimensional region to be modeled by combining the elements developed in the previous phase; 3) Determining the radiance field around each element of the modeled environment by employing an iterative, relaxation technique to diffuse the source radiance throughout the environment; 4) Displaying the results of the model numerically and graphically. The final objectives are to evaluate and validate the model results with field radiance and irradiance data for a variety of settings, and to apply the model to predicting the perceptibility of underwater objects for all angles and fields of view.

APPROACH

Consider a point, $\boldsymbol{\rho_i}$, on the surface of an arbitrary region (Fig. 1). This point is being illuminated by a pencil of radiant power, E_i, at wavelength λ_i and from direction $\boldsymbol{\varepsilon_i}$. E_i is that portion of the irradiance at $\boldsymbol{\rho_i}$ that arrives from direction $\boldsymbol{\varepsilon_i}$, expressed in units W m^{-2} sr^{-1}. As a result of this illumination, power may be emitted from the region at wavelength λ_o, point $\boldsymbol{\rho_o}$, and direction $\boldsymbol{\varepsilon_o}$. In the following

Report Documentation Page

Form Approved
OMB No. 0704-0188

1. REPORT DATE	2. REPORT TYPE	3. DATES COVERED
30 SEP 2006		**00-00-2006 to 00-00-2006**

4. TITLE AND SUBTITLE	5a. CONTRACT NUMBER
Optical Variability and Bottom Classification in Turbid Waters: HyMOM Predictions of the Light Field in Ports and Beneath Ship Hulls	5b. GRANT NUMBER
	5c. PROGRAM ELEMENT NUMBER
6. AUTHOR(S)	5d. PROJECT NUMBER
	5e. TASK NUMBER
	5f. WORK UNIT NUMBER
7. PERFORMING ORGANIZATION NAME(S) AND ADDRESS(ES) **University of South Florida,College of Marine Science,140 Seventh Ave. South,St. Petersburg,FL,33701**	8. PERFORMING ORGANIZATION REPORT NUMBER
9. SPONSORING/MONITORING AGENCY NAME(S) AND ADDRESS(ES)	10. SPONSOR/MONITOR'S ACRONYM(S)
	11. SPONSOR/MONITOR'S REPORT NUMBER(S)

12. DISTRIBUTION/AVAILABILITY STATEMENT
Approved for public release; distribution unlimited

13. SUPPLEMENTARY NOTES

14. ABSTRACT

15. SUBJECT TERMS

16. SECURITY CLASSIFICATION OF:			17. LIMITATION OF ABSTRACT	18. NUMBER OF PAGES	19a. NAME OF RESPONSIBLE PERSON
a. REPORT **unclassified**	b. ABSTRACT **unclassified**	c. THIS PAGE **unclassified**	**Same as Report (SAR)**	**10**	

discussion we will omit for simplicity specific reference to wavelength dependence, and we also defer treatment of internal sources, as the extension of the technique to include these phenomena is straightforward. Surface reflectance, however, is included in the following formulation.

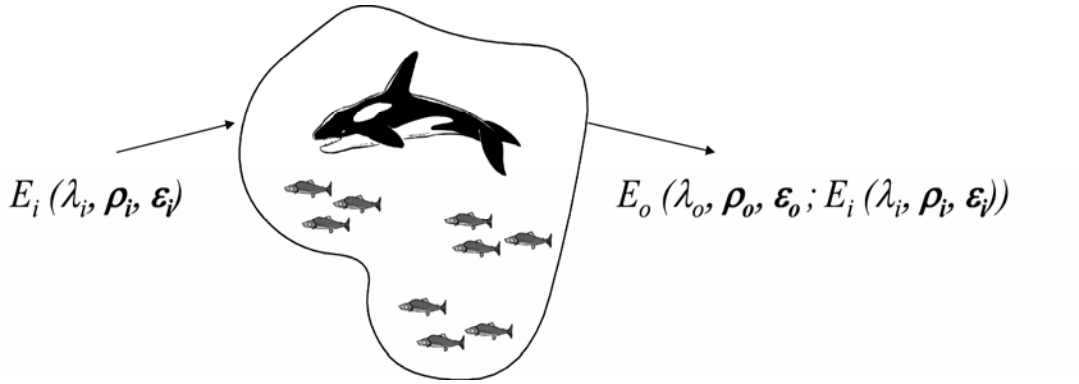

Figure 1: $E_o(\lambda_o,\boldsymbol{\rho}_o,\boldsymbol{\varepsilon}_o;E_i(\lambda_i,\boldsymbol{\rho}_i,\boldsymbol{\varepsilon}_i))$ is the part of the irradiance emitted from the region at wavelength λ_o, point $\boldsymbol{\rho}_o$, and direction $\boldsymbol{\varepsilon}_o$ when the region is illuminated by irradiance incident at wavelength λ_i, point $\boldsymbol{\rho}_i$, and direction $\boldsymbol{\varepsilon}_i$. [The figure gives a graphic representation of the equations which follow].

The linearity of the Radiative Transfer Equation (RTE) implies that $E_o(\boldsymbol{\rho_o},\boldsymbol{\varepsilon_o};E_i(\boldsymbol{\rho_i},\boldsymbol{\varepsilon_i}))$ is proportional to $E_i(\boldsymbol{\rho_i},\boldsymbol{\varepsilon_i})$. We denote the point-by-point constant of proportionality as the "response function" (RF), defined as

$$E_o(\boldsymbol{\rho_o},\boldsymbol{\varepsilon_o};E_i(\boldsymbol{\rho_i},\boldsymbol{\varepsilon_i})) \;=\; R(\boldsymbol{\rho_o},\boldsymbol{\varepsilon_o};\boldsymbol{\rho_i},\boldsymbol{\varepsilon_i})E_i(\boldsymbol{\rho_i},\boldsymbol{\varepsilon_i}). \qquad (1)$$

Now, if R is known for all points on the boundary of the region, and for all directions, then the power emitted by the region is completely determined by the incident power distribution. The total power emitted from the differential of surface area centered on $\boldsymbol{\rho_o}$ and propagating within the differential cone of directions centered on $\boldsymbol{\varepsilon_o}$ is given by

$$E_o(\rho_o,\varepsilon_o)dA(\rho_o)d\Omega(\varepsilon_o) = \iint R(\rho_o,\varepsilon_o;\rho_i,\varepsilon_i)E_i(\rho_i,\varepsilon_i)\,dA\,d\Omega\,. \qquad (2)$$

The integrals in (2) are over the entire boundary of the region and all directions, $d\boldsymbol{\Omega}$, which are incident on the region at $dA(\boldsymbol{\rho_o})$.

The relationships given in (1) and (2) are not very useful (except to Monte Carlo programmers), but do warrant two comments. First, R is a relationship between points on the surface of the region and is not explicitly dependent on the optical media within. Of course, R does depend on the material within the region. But if R can be measured, deduced, or defined for the region, then whenever the power distribution incident on the surface of the region is known, the emitted power distribution can be calculated without further reference to the optical properties of the region. Secondly, there actually are regions for which R is known or may be defined exactly. These include regions within which no scattering takes place and boundary regions that have known reflectance characteristics.

The approach used in the preliminary stages of this work was to model two-dimensional elements such as infinitely long bars of square and right-triangular cross-section using Monte Carlo techniques. Once

a collection of response functions was developed to represent the optical characteristics of the environment to be modeled, the elements (e.g. cubes; surfaces) were assembled by means of adjacency relationships to represent the geometric characteristics of the environment. Then, for each element in the model environment, the radiant input to the element from adjacent elements is determined, and the output state of the element is adjusted according to the element's response function. This process is repeated for all elements in the environment until the change in elemental output states is negligible. At this point the radiance field on the boundary of each element is known.

WORK COMPLETED

HyMOM models of one, two, and three dimensions have been developed and applied to modeling of natural light fields about ridges and trenches and beneath ships (2-D; Reinersman and Carder, 2004) and around pilings (3-D small environment; Carder et al. 2005). Extension of HyMOM to 2 wavelengths (305 nm and 532 nm) and a larger 3-D field (10m x 10m x 5m) with a 5m cubic object (e.g. mine or coral head) illuminated by sun and skylight was reported at Ocean Optics XVIII (Carder et al. 2006; Figs. 3, 4). Finally, the perceptibility from different directions of a high-contrast deep (10m) object on the bottom and AUVs flown 2m and 8m above a 10m bottom with zero contrast to the environment are simulated. Shadows provide the only contrast with the environment. The two AUVs are then switched in altitude with no change in contrast. Again the perceptibility with view angle is evaluated. Preliminary results are shown below.

RESULTS

We have successfully developed and deployed the Real-Time Ocean Bottom Optical Topographer (ROBOT) (Carder et al. 2001; Carder et al. 2003; Carder et al. 2005) to map bottom substrates and natural and foreign objects found on them. In particular, bottom mines and hull limpet mines have been clearly delineated by a combination of their three-dimensionality and their albedo contrast.

Predicting the conditions under which ROBOT and other optical sensors are able to perform as expected depends upon two optical models: 1) an environmental optical model; and 2) a sensor performance model. 2-D and 3-D environmental optical models have been developed (Reinersman and Carder 2004) and tested (Carder et al, 2005) that calculate the radiance field in all three directions with ca. 5-10 degree angular and 12.5 cm spatial resolutions. The feasibility of observing the ROBOT laser fan beam on the bottom of a ship hull in daylight from various ranges can be determined (Reinersman and Carder 2004; Carder et al. 2005; Montes-Hugo et al. 2005; Montes-Hugo 2005). The greater the range, the faster a hull can be inspected using a fan beam. A sensor model was also developed here last year (Montes-Hugo and Carder 2005; Montes-Hugo 2005). We plan to combine the techniques in continuing work. This year the model has been expanded to a larger three-dimensional environment to evaluate the perceptibility of bottom objects and AUVs under natural lighting conditions.

Bottom-object problem:

1) The modeled environment is a cubic region of water 10m on a side (Fig. 2). The surface is flat and Fresnel reflection is included in the simulation. The water column is homogeneous, and the bottom is flat, except for a half-meter cubic box located on the bottom near the middle of the modeled region. The box is "dark", in contrast to the "bright" bottom (specific optical parameters follow.) The bottom of the region and the sides and top of the object box are modeled as Lambertian reflectors. Photons departing the modeled region through lateral boundaries are

allowed to “wrap around”. Therefore, the effective modeled region is an infinite slab of water 10m deep, with a square lattice of half-meter cubes placed on the bottom on 10m centers.

2) Numerical parameters:

Total number of elements in simulation, including source, surface, and bottom “plates”, cubic water elements, and box sides and top: 9203

Spatial resolution: half-meter boxes and plates with 4 counting cells per face.

Angular resolution: 12 “theta bins” / 90 degrees, 48 “phi bins” / 360 degrees, yielding 7.5 degree resolution in both directions.

Source geometry: solar zenith angle=41.25 degrees; Solar azimuth angle=3.75 degrees

a(water) = .05172/m	(532 nm)	c(total) = .211784/m
a(part) = .0130405/m		vsf(water) – Rayleigh
b(water) = .00218/m		vsf(part) – Mobley’s Petzold
b(part) = .144844/m		Total, effective Bb/B = .025272
a(total) = .0647605/m		Reflectance(bottom) = .25
b(total) = .147024/m		Reflectance(box) = .05

3) Results of 1-d comparison of typical column with Mobley’s Hydrolight:

Eu(0+): -1.47 % ((model - Hydro)/Hydro) * 100
Eu(0-): -3.45%
Ed(-10m): -1.44%

The perception of an object is a function of its contrast to the surrounding radiant environment and the path radiance between an object and the viewer. The contrast of an object on the bottom diminishes with range (Fig. 2), and the light field on the bottom on all sides adjacent to a proud object diminishes due to shade of the diffuse light field by the object.

HyMOM was also used to calculate fractions of the surface irradiance reaching a cubic “coral head” on a 5m bottom as shown in Figures 3, and 4 at 305 and 532 nm, representing the UVB and visible spectra, respectively (Carder et al. 2006). The underwater solar zenith angle for this Florida Keys scenario is 28.9^{o}. The solar azimuth is in the first angular bin 3.75^{o} north of due east. The subsequent shadow on the seabed falls just south of west and is nearly as dark on the south face as on the west face of the cube. The fraction of visible surface irradiance hitting the shaded, west face of the “coral head” is 25% that hitting the sunny, east face. For UVB it is nearly twice as large at 47% (Figs. 1b, 2b). This is because the diffuse fraction of $E_d(0+,305)$ is thrice that of $E_d(0+,532)$. Thus UVB (305 nm) is a much more significant part of shadow-infilling by the diffuse field than is the visible irradiance. This suggests that behavioral cueing based on PAR (e.g. coral sunscreen synthesis or motility of foraminifera to optimize photosynthesis) may cause UVB over-dosing even on the shady side of coral heads for ENSO and/or volcanic-like conditions when the ozone layer thins and CDOM bleaches (Carder et al. 2006). Examination of the spectral nature of the structural light field around coral heads and other vertical structures should be included in future studies of bleaching of coral and foraminifera.

UUV camouflage problem

A coating that matches the albedo of the diffuse upwelling light field makes a near-bottom, cubic, diffuse object nearly imperceptible to an aircraft sensor flying with the sun behind it since all solar shadows are lost. However, HyMOM was used to view a horizontal cylinder (e.g. AUV) of 0.5m diameter and 3m long with a diffuse, Lambertian coating and albedo matching the irradiance reflectance of the undisturbed water column. At 2m above a 10m bottom, the AUV was nearly invisible (Fig. 5a), with only a 2.6% contrast. At 8m above the bottom, the AUV with an irradiance-matching albedo was quite visible (Fig. 5b), with a 16.2% contrast. Why?

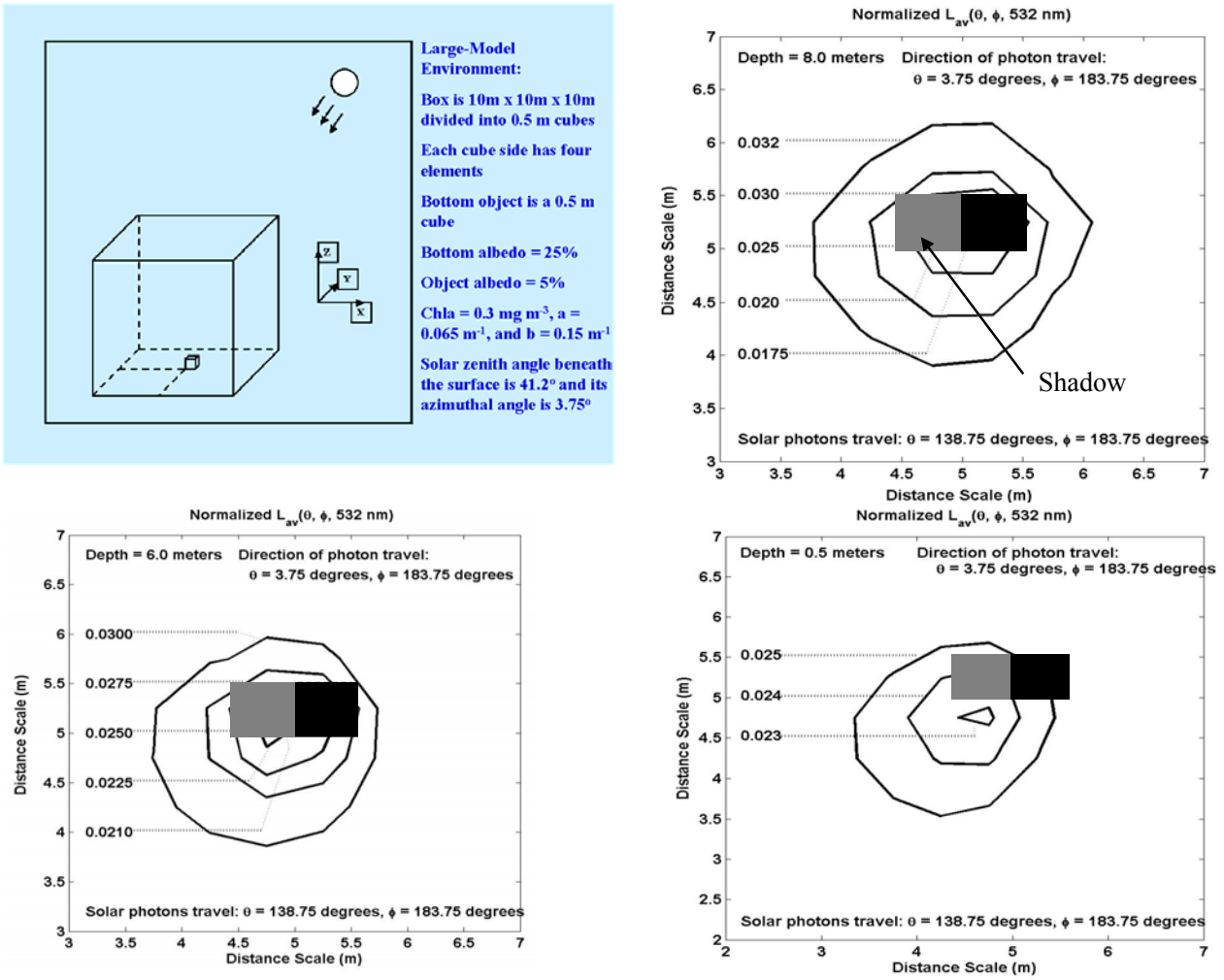

Figure 2. The model environment (upper left) followed by the radiance field viewed at a 3.75° nadir and 3.75° azimuth angle from 2 m, 4 m, and 9.5 m above the bottom. Note the diminution in the contrast with height, going from 29.3% at 2 m height to 4.1% at 9.5 m height. Path radiance and angular resolution both contribute to reduced contrast. Note that diffuse sky and water irradiance reaching the bottom is diminished on all sides of the cube (e.g. @2m) causing uniform shade, while solar shadow on the left. Path radiance in-fills the solar shadow last.

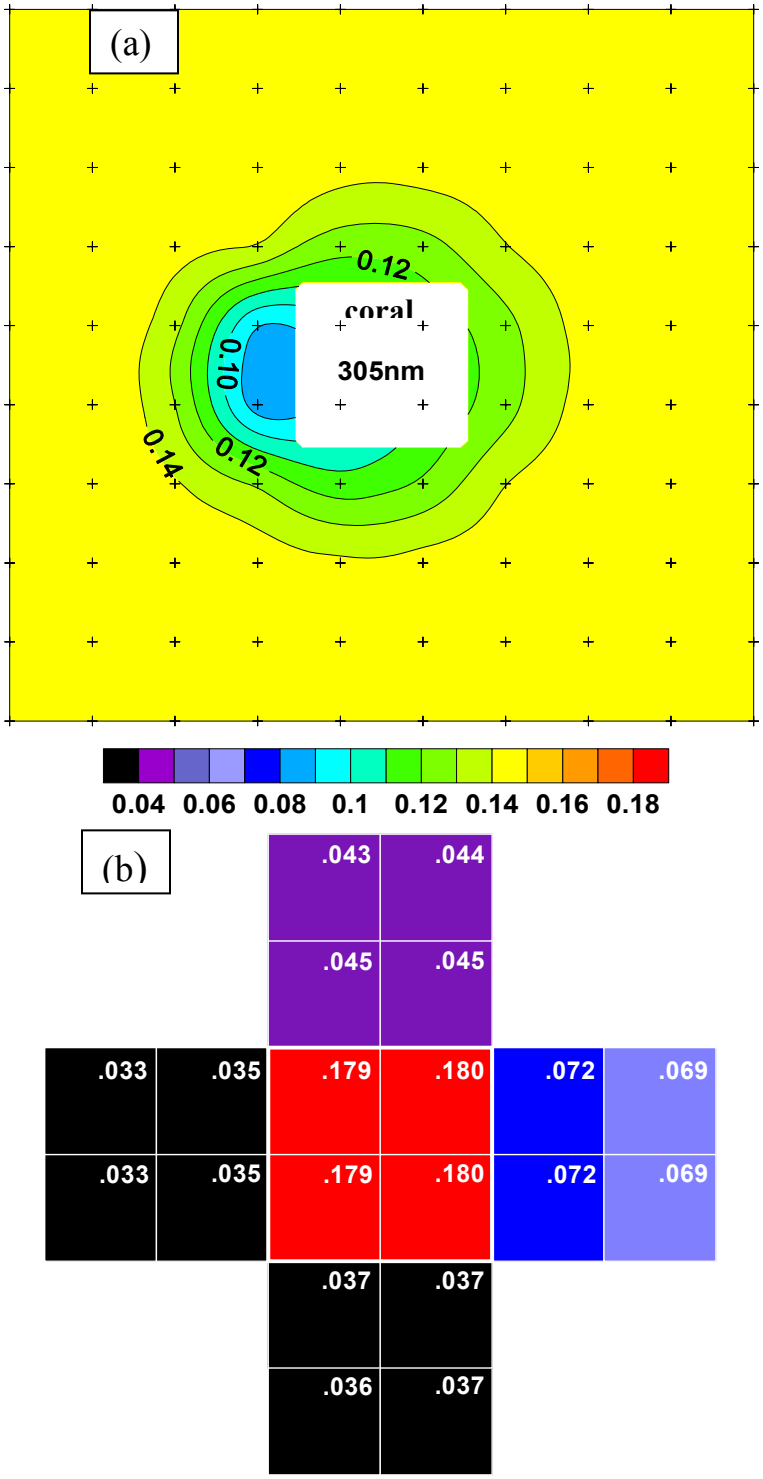

Figure 3. Plan view of HyMOM simulations of the fraction of surface irradiance $E_d(0^+,305)$ hitting each of the 0.25m facets of: (a) the sea floor at 5 m depth; and (b) view of the top (center) and four sides of the "coral head". Sub-aerial solar zenith angle is 40^o, azimuth angle is 3.75^o north of due east, and "+" marks are at the centers of the 100 model panels for the seafloor.

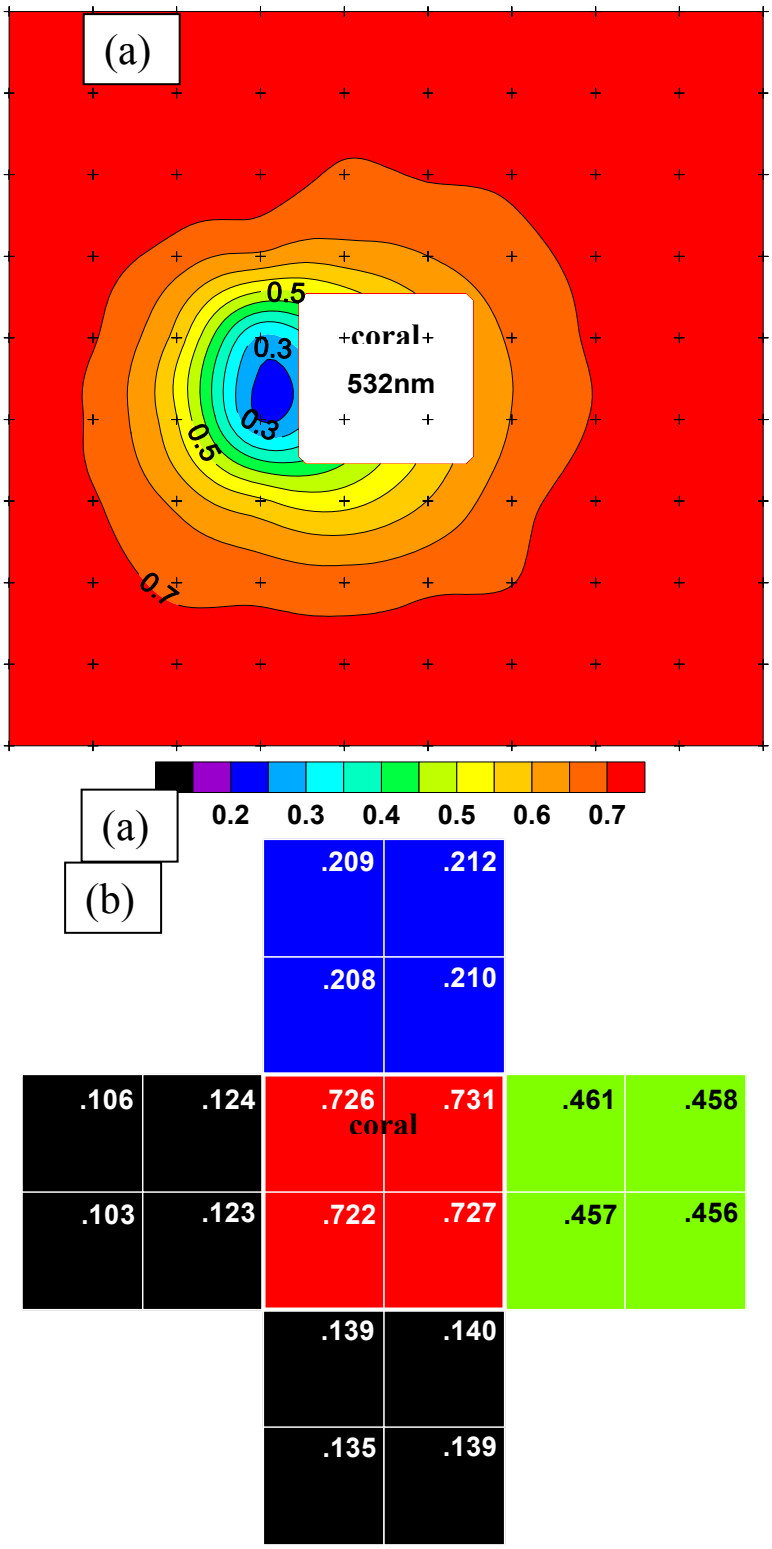

Figure 4. HyMOM simulations of the fraction of surface irradiance $E_d(0^+,532)$ hitting each of the 0.25m facets of: (a) the sea floor at 5 m depth; and (b) the top and four sides of the "coral head". The sub-aerial solar zenith angle is 40^o, the solar azimuth angle is 3.75^o north of due east, and "+" marks are at the centers of the 100 model panels for the seafloor.

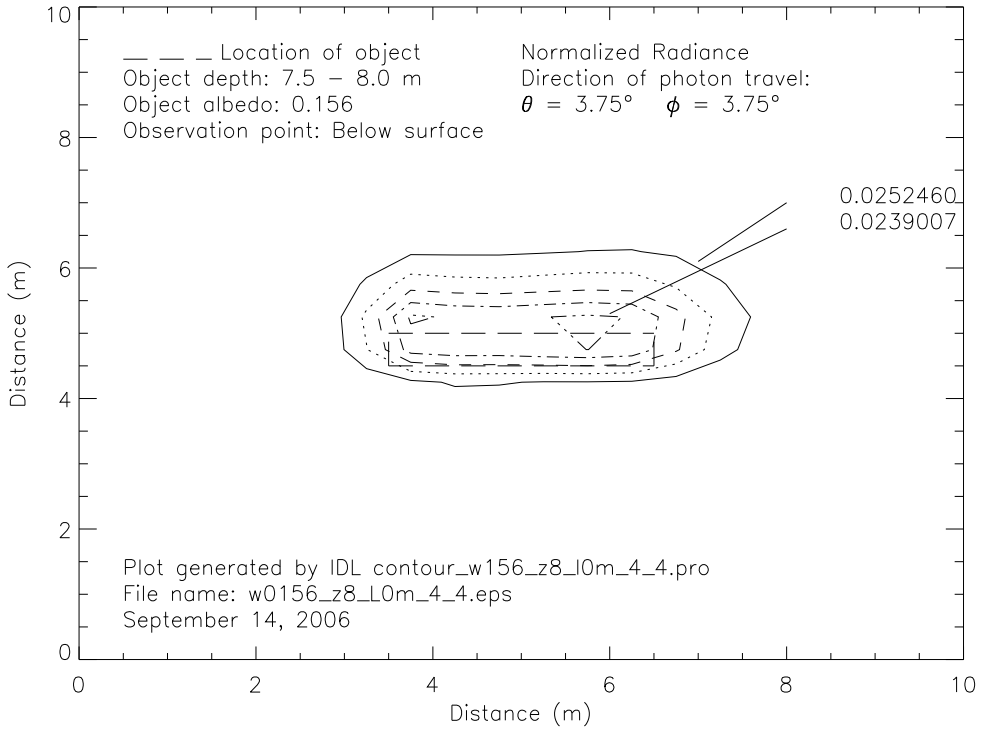

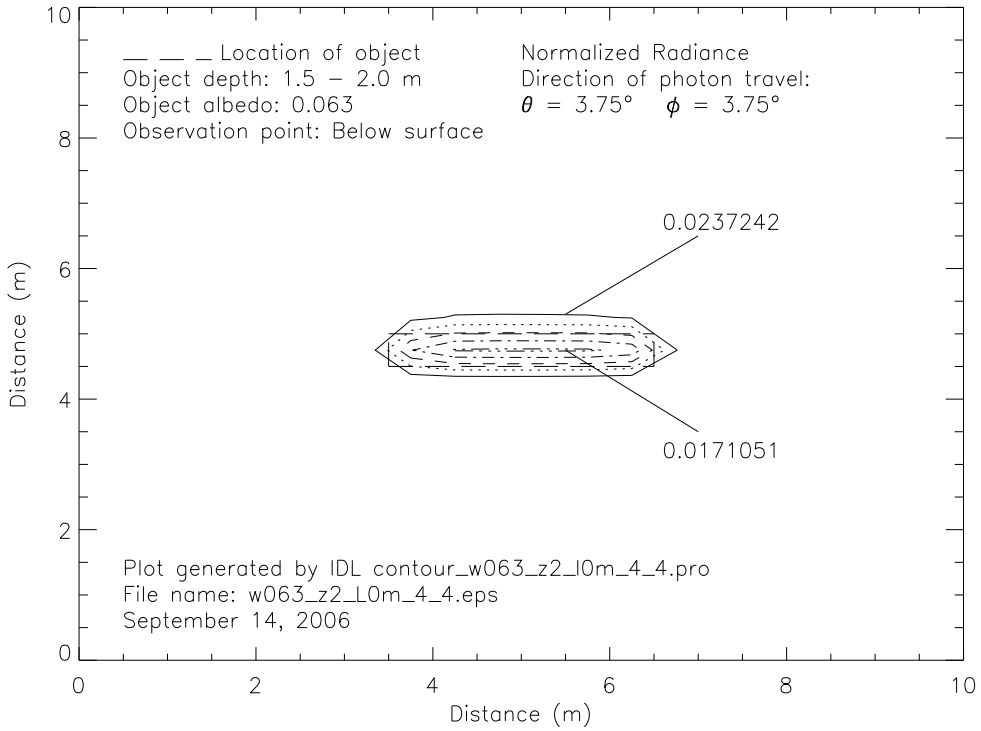

Figure 5. Cylindrical AUV viewed from a subsurface, nadir perspective: a) AUV diffuse albedo = 0.156 and altitude 2m above a 10m bottom; b) AUV diffuse albedo = 0.063 and altitude 8m above a 10m bottom .[See text for discussion]

A number of subtle factors interplay in these results: 1) The Q factor (E_u/L_u) is pi for the diffuse, Lambertian bottom and AUV albedo, but approaching the surface, the light field is brightest at nadir with Q=2.21. The light field occluded by the AUV near the bottom is nearly Lambertian, so its diffuse coating is a good match. With a near-surface, nadir view, the AUV occludes a brighter radiance field in the upward direction than it replaces by diffuse reflectance, making its image appear darker than the medium. 2) Its cylindrical shape reflects a significant fraction of light downward from its curved top rather than only upward, reducing its effective albedo even more and increasing its contrast to 16.2%. 3) Viewing the AUV from an oblique subsurface angle of 26^o, however, did reduced its contrast to 13.0% as expected from the Q-factor argument, but this only compensated in part for the Q-factor effect and did nothing to alleviate the downward reflection bias of its curved top surface.

Snell's Law severely limits the obliquity of source and view zenith angles for observations from an aircraft since all light traveling upward in water with a zenith angle greater than 49^o is internally reflected at the sea surface. This provides a mostly top view of objects observed from the sky. If nadir view angles in air have a practical limit of about 53^o (Brewster's polarization angle) for removal of reflected skylight (e.g. Neville and Gower 1977; Fougnie et al. 1999), then the optimal subsurface nadir view angle would be about 37^o. Thus, the Q factor effect must be considered for subsurface nadir view angles from 0^o to 37^o for any camouflage and detection schemes.

We suspect that an AUV would be less easily detected, especially near the surface, if its top surface were flat (AUV either rectangular or triangular in cross section), and if its coating better matched the non-diffuse character of the water column with depth. This perhaps argues for an active cloaking system. Otherwise, for nadir views, it must have a brighter, diffuse albedo than the irradiance reflectance of the water column observed at a given depth, and it must remain at that depth for a given water column.

SUMMARY

•Laser-line model developed and published
•2-D and 3-D optical environments modeled
–Barge problem: simulated, validated, published
–Pilings: simulated and published
–Bottom object: simulated and discussed; published for UVB effects on coral bleaching
–Perceptibility problem begun for AUV @2m and @8m above 10m bottom
  –Higher resolution and higher-speed calculations (e.g. more computational power) will improve model accuracy

COLLABORATIONS:

- Compact Optical Imager for Real-time, 3-D Range, Intensity and Fluorescence Mapping of the Ocean Floor (N00014-01-1-0279: Kaltenbacher et al. [USF/COT/CMS]

- Advanced Underwater Port Security Systems (N00014-02-1-0859: Kloske [USF/COT] and Tripp [USCG])

- Development of a Mobile Inspection Package (N00014-03-1-0708: Kloske [USF/COT] and Tripp [USCG])

- Testing and Evaluation of the Mobile Inspection Platform (N00014-03-1-0750: Kloske [USF/COT] and Tripp [USCG])

- Quantifying HAB Concentrations and Chlorophyll a in Coastal Waters, NASA grant to K.L. Carder.

REFERENCES

Carder, K.L., D.K. Costello, L.C. Langebrake, W. Hou, J.T. Patten, and E.A. Kaltenbacher. 2001. Real-time AUV data for command, control, and model inputs. *IEEE Jour. of Ocean Eng.*, 26(4), 742-751.

Carder, K.L.,C.C. Liu, Z. Lee, D.C. English, J.Patten, F.R. Chen, J.E. Ivey, and C. Davis. 2003. Illumination and turbidity effects on observing facetted bottom elements with uniform Lambertian albedos. *Limnol. Oceanogr.*, 48(1), 355-363.

Carder, K.L., P. Reinersman, D. Costello, J. Kloske, and M. Montes, 2005. Optical Modeling of Ports and Harbors in 2 and 3 Dimensions, in *SPIE Proceedings 5780(49)*, 10pp.

Carder, K.L, Reinersman, P.N.; Hallock, P., 2006. A 3-D model of light effects related to the bleaching of corals and foraminifera, Ocean Optics XVIII, Montreal (extended abstract on CDROM, ONR, Arlington, VA).

Fougnie, B., R. Frouin, P. LeCompt and P.Y. Deschamps, 1999. Reduction of skylight reflection effects in the above-water measurement of diffuse water marine reflectance, *Appl. Opt. 38*: 3844–3856.

Montes-Hugo, M.A., 2005. *Monte Carlo simulations as a tool to optimize target detection by AUV/ROV laser line scanners*, M.S. thesis, University of South Florida, Tampa, Florida.

Montes-Hugo, M.A. and K.L. Carder, 2005. Monte Carlo simulations as a tool to optimize target detection by AUV/ROV laser line scanners, *SPIE Proceedings 5799(1)*, 12 pp.

Neville, R.A. and J.F.R. Gower, 1977. Passive remote sensing of phytoplankton via chlorophyll a fluorescence. *J. Geophys. Res.* 82: 3487-3493.

Reinersman, P. N. and K. L. Carder. 2004. Hybrid Numerical Method for Solution of the Radiative Transfer Equation in One, Two, or Three Dimensions. *Appl. Opt.* ***43***: 2734-2743